

# Federated Neural Radiance Fields

Lachlan Holden, Feras Dayoub, David Harvey, Tat-Jun Chin  
 Australian Institute for Machine Learning  
 The University of Adelaide, SA 5005, Australia

{lachlan.holden,feras.dayoub,david.harvey,tat-jun.chin}@adelaide.edu.au

## Abstract

The ability of neural radiance fields or NeRFs to conduct accurate 3D modelling has motivated application of the technique to scene representation. Previous approaches have mainly followed a centralised learning paradigm, which assumes that all training images are available on one compute node for training. In this paper, we consider training NeRFs in a federated manner, whereby multiple compute nodes, each having acquired a distinct set of observations of the overall scene, learn a common NeRF in parallel. This supports the scenario of cooperatively modelling a scene using multiple agents. Our contribution is the first federated learning algorithm for NeRF, which splits the training effort across multiple compute nodes and obviates the need to pool the images at a central node. A technique based on low-rank decomposition of NeRF layers is introduced to reduce bandwidth consumption to transmit the model parameters for aggregation. Transferring compressed models instead of the raw data also contributes to the privacy of the data collecting agents.

## 1. Introduction

Neural radiance fields (NeRF) [13] are a recently developed neural network model that are proving to be a powerful tool for 3D modelling. Trained on a finite set of image observations of a scene with ground truth camera poses, the output of a NeRF can be used to synthesise photo-realistic images from previously unseen viewpoints of the scene. While originally applied to object-centric scenes, there is increasing work on using NeRFs to model outdoor environments [21,22,26]. This could contribute to capabilities such as augmented reality and autonomous navigation.

Existing NeRF methods mostly take a *centralised learning* paradigm, which requires all training images to be available on a single compute node before the training of NeRF can proceed. On the other hand, many researchers have advocated using multiple agents (*e.g.*, tourists, cars, UAVs) to cooperatively collect data from outdoor environ-

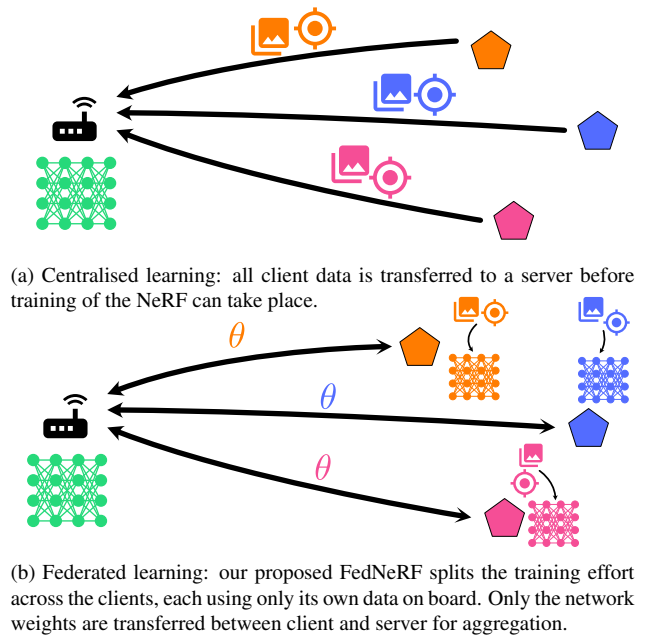


Figure 1. Centralised versus federated learning of NeRF.

ments [6, 10, 11]. Employing this data collection approach to environment modelling using NeRF entails transferring all collected images to a central node (see Fig. 1a), which can incur high data communication costs. Moreover, the privacy of the data collectors is not guaranteed due to the sharing of the data to a central pool.

As edge computing devices increase in processing capability [11, 16], it has become practical to perform neural network optimisation on the edge. If the effort to train an overall model can be distributed and parallelised across multiple edge devices, particularly if each device needs to take into account only the data that is on board, the potential to speed up training convergence of the overall model is significant. In addition, the need to pool the data is alleviated.

Towards collaborative sensing and learning of NeRF for scene modelling, the main question we ask in this paper is: *Can a NeRF be learned in a parallel and distributed manner across multiple compute nodes, without pooling the data?*

**Contributions.** We answer the question in the affirmative by developing a novel federated learning algorithm for NeRF, called **FedNeRF**. Our experiments validate that the structure of traditional MLP-based NeRF is amenable to optimisation across multiple compute nodes using standard federated averaging techniques, where each node tunes the model using an independent set of image observations of the overall scene. To reconcile the resultant models at the different nodes, only the optimised weights need to be communicated to a central node for aggregation into an overall NeRF; see Fig. 1b.

To reduce bandwidth consumption during the update cycles of FedNeRF, we introduce a simple model reparametrisation technique based on low-rank approximation to reduce the number of effective parameters in NeRF. Results show that this compresses *each* weight update by as much as 65% (resulting in total bandwidth reduction of 97.5%) without greatly affecting the accuracy of the learned NeRF, indicating a high level of redundancy in the model.

**Benefits.** FedNeRF is able to leverage multiple compute nodes to speed up training convergence of NeRF. In the context of multi-agent sensing and learning, FedNeRF incurs smaller data communication costs due to the low-rank compression applied on the NeRF weights. Transferring the compressed models and avoiding data sharing and pooling also help maintain the privacy of the data collection agents.

## 2. Related work

NeRF is a relatively new technique [13] that is receiving a lot of attention in the vision community. Here, we survey recent advances that are relevant to the proposed FedNeRF.

### 2.1. NeRF

A NeRF is a neural network that implicitly represents a 3D scene in that a NeRF can accurately render arbitrary views of the scene. A NeRF model is a much more compact (*e.g.*, 5 MB [13]) than storing all the training images or other conventional 3D model representations. More technical details of NeRF will be presented in Sec. 3.

To improve the robustness of NeRF against imaging conditions (*e.g.*, lighting, exposure) and transient occlusions (*e.g.*, pedestrians, cars), NeRF in the Wild (NeRF-W) [10] includes a learned appearance embedding for each image for the colour-generating part of the network. Transient occlusions are handled by adding a new transient head to the model with a second learned embedding that generates an uncertainty field alongside a transient colour and density.

Standard NeRF works well for object-centric and indoor scenes but is less capable of modelling outdoor scenes with far-away backgrounds. NeRF++ [29] addresses this by using two NeRFs; one modelling the foreground objects in a

unit sphere, and the other using an inverted sphere reparametrisation to represent everything outside the sphere.

DeRF [17], and KiloNeRF [18] also decompose a NeRF into multiple sub-NeRFs, but to improve the rendering time. DeRF uses a modest number of sub-networks split using learned Voronoi decomposition, while KiloNeRF uses a large number of small, efficient NeRFs in a spatial grid.

### 2.2. Large-scale NeRF

Scaling up NeRF to represent large scenes (*e.g.*, streetscapes) while retaining fine details is an active research topic with potential applications in localisation and navigation [15, 28]. It has been found that simply increasing the network size has diminishing returns on the quality of synthesised images for more complex scenes [17]. More successful approaches conduct spatial or geometric decomposition to model a large scene using a collective of NeRFs.

To model a city block, Block-NeRF trains a set of NeRFs distributed in and between city block intersections [21]. Each NeRF is trained on the set of training images with camera pose within a certain radius of some training area origin. At inference time, the final image is created by combining the rendered images of each NeRF whose training area includes the query pose. Instead of partitioning the training data by full image based on the pose of the camera as in Block-NeRF, in Mega-NeRF [22] each *pixel* is included in the train sets for each NeRF whose area its ray intersects. At inference time, the rendered image is created by combining the outputs of each NeRF whose area is intersected by the ray of each pixel. Instead of separating NeRFs spatially, BungeeNeRF creates progressively larger models with segmented training data of multiple scales to be able to render high-quality outputs in larger scenes at a range of distances and resolutions [26]. It is based on Mip-NeRF [2], which uses conical frustums rather than rays to represent pixels to better render fine details at high resolutions.

**Contrasting FedNeRF with large-scale NeRF.** We stress that FedNeRF solves a task that is orthogonal to that addressed by large-scale NeRF techniques [21, 22, 26]. While large-scale NeRFs decompose the *scene* into separate cells where each is modelled by an individual NeRF, FedNeRF distributes the *data* (or *data collection effort*) and *model optimisation* over multiple clients.

Combining FedNeRF with large-scale NeRF techniques is possible, which we leave as future work.

### 2.3. Federated learning

Federated learning is a mechanism by which multiple agents cooperating can train a single neural network in a shared way [7, 11, 12]. There is a single central server node and a number of client nodes. Training is performed distributed over the clients on data collected by each client,

and this data does *not* need to be sent to the server – instead, only network weights are transferred back and forth.

Due to the need to transfer network weights, reducing bandwidth usage in federated learning is important. Techniques include distributed optimisation [14], client dropout [3, 25], update compression via techniques like sparsification and quantisation [1, 9, 14, 19, 20, 27], and intermediate update aggregation [5]. Another technique, and the one adopted by our work, involves reparameterising the model to yield fewer effective weights [4, 8].

While federated learning is a mature topic, we are the first to adapt it to NeRF and achieve concrete results in collaborative multi-agent sensing and modelling.

### 3. Preliminaries

Here, we provide a brief introduction to NeRF; the reader is referred to [13] for more details. In its original form, a NeRF is a fully-connected neural network with intermittent skip connections that map a 5D input, consisting of a 3D point in the scene  $\mathbf{x} = (x, y, z)$  and the pitch and yaw of a viewing direction  $\mathbf{d} = (\beta, \phi)$ , into a density  $\sigma$  and RGB colour  $\mathbf{c} = (r, g, b)$ . A synthetic image of the scene can be rendered through traditional volume rendering techniques by sampling colour and opacity from the network at numerous points along rays through the scene.

A NeRF first predicts  $\sigma$  solely from  $\mathbf{x}$ , and then this output is concatenated with  $\mathbf{d}$  and fed to the second part of the network to predict  $\mathbf{c}$ . Additionally, two networks are actually trained simultaneously – a coarse and fine network pair. The output of the coarse is used during rendering to inform the samples taken from the fine network. To enable the networks to represent high-frequency features in the scenes, the inputs are first transformed by a positional encoding.

The parameters of a NeRF can be defined as  $\theta = \{\mathcal{W}, \mathcal{B}\}$ , where  $\mathcal{W} = \{\mathbf{W}_1, \mathbf{W}_2, \dots\}$  are matrices representing the weights of the fully connected (FC) layers, and  $\mathcal{B} = \{\mathbf{b}_1, \mathbf{b}_2, \dots\}$  are the corresponding bias vectors. Note that for a single NeRF, these sets include the parameters for both the coarse and fine networks together.

A NeRF is trained on a dataset  $D = \{(I_\ell, p_\ell)\}_{\ell=1}^N$  consisting of images  $I_\ell$  of a scene and corresponding poses  $p_\ell$ . In each iteration of the training, a batch of pixels are randomly sampled from a selected image  $I_\ell$ . For each pixel ray, the network is queried as in inference to render a pixel colour, and the mean squared error (MSE) between this colour and the ground-truth pixel colour is employed as the training loss to update the network parameters  $\theta$ .

### 4. Application scenario

Consider  $K$  agents (a.k.a. clients) that work collaboratively to map a scene. The clients are equipped with sensors and edge compute devices, and can communicate with

a central server. The clients collect images of the scene with ground truth poses derived from onboard positioning systems; this requirement is realistic for platforms such as vehicles and UAVs (*cf.* [6, 11, 22]). Let  $D_k$  be the data collected by the  $k$ -th client. The overall aim is to learn a NeRF  $\theta$  using all the data collected  $\{D_k\}_{k=1}^K$ . Fig. 2 illustrates.

For brevity, the scenario description considers only one data collection round. However, the methods in the rest of the paper can be executed sequentially to handle multiple rounds, *e.g.*, to conduct lifelong mapping [6, 24].

**Baseline method.** Given initial NeRF weights  $\theta^{(0)}$  (*e.g.*, the estimate on previously collected data or on an arbitrarily chosen  $D_k$ ), the baseline method (Alg. 1) involves each client sending the recorded data back to the server. The initial  $\theta^{(0)}$  is then refined at the server using all collected data.

The bandwidth consumption of the baseline method is

$$B_{\text{baseline}} = \sum_k |D_k|, \quad (1)$$

where  $|D_k|$  is the size of data  $D_k$  as the number of bytes. In practice,  $B_{\text{baseline}}$  is significant due to transferring raw images (even with JPEG compression). Moreover, the baseline method does not fully exploit the compute power of the clients, and can lead to slower convergence than distributed optimisation, as we will show in Sec. 6.2.

---

Algorithm 1. Baseline method for the application scenario (Sec. 4). Data transfers are marked by \*.

---

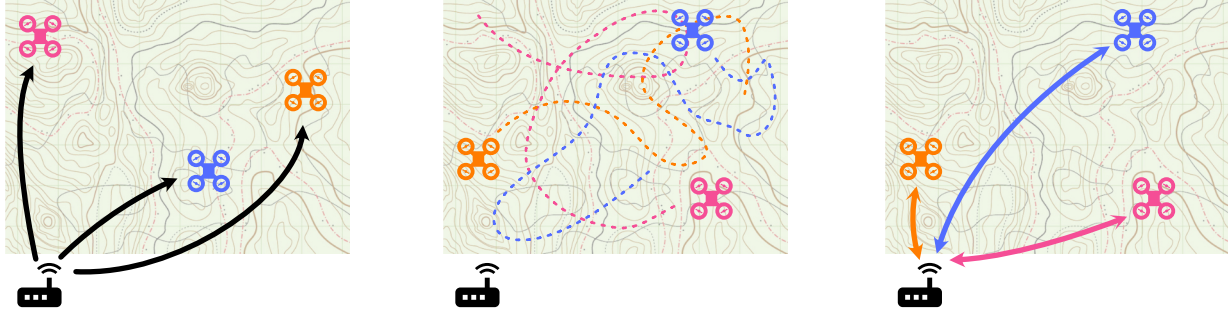
**Hyperparameters:**

- Number of training iterations  $T$
  - 1  $\theta^{(0)}$  are initial NeRF weights
  - 2 **for** client  $k \leftarrow 1, \dots, K$  **do** ▷ *parallel loop*
  - 3      $D_k$  is data collected by client  $k$
  - 4      $D_k$  is transmitted to the server \*
  - 5 **end**
  - 6  $\theta^{(1)} \leftarrow \text{Train-NeRF}(\theta^{(0)}, \{D_k\}_{k=1, \dots, K}, T)$   
▷ *standard NeRF training; see Sec. 3*
  - 7 **return**  $\theta^{(1)}$
- 

### 5. FedNeRF

The proposed FedNeRF is summarised in Alg. 2 and illustrated in Figs. 1b and 2. The main distinguishing features of FedNeRF from the baseline method are:

- The sharing of NeRF weights to each client which are then refined onboard using collected data.
- The transfer of the individual refined weights back to the server to be aggregated into an overall model.
- The compression of updates through a low-rank model reparameterisation technique to reduce bandwidth consumption due to the transfer of the weights.



(a) Receive initial weights from the server. (b) Take new photos and update individual NeRFs. (c) Aggregate weights with server.  
 Figure 2. Main steps of FedNeRF, framed in an example application scenario of mapping an outdoor area with a fleet of quadcopters.

It is vital to note that the **for** loop in Steps 9 to 13 is *executed in parallel* on the clients. Also, Alg. 2 can be executed sequentially for lifelong mapping. The rest of this section will provide more details of the major steps in Alg. 2.

---

Algorithm 2. Proposed FedNeRF for the application scenario (Sec. 4). Data transfers are marked by \*.

---

**Hyperparameters:**

- Variance  $\alpha$
- Number of merge rounds  $M$
- Number of training iterations per merge  $\Upsilon$

```

1  $\theta^{(0)} = \{\mathcal{W}^{(0)}, \mathcal{B}^{(0)}\}$  are initial NeRF weights
2  $\mathcal{L}^{(0)}, \mathcal{R} \leftarrow \text{Reparameterise}(\mathcal{W}^{(0)}, \alpha) \triangleright$  these are
   the learnable and frozen parameters; see Sec. 5.2
3  $\mathcal{C}^{(0)} \leftarrow \{\mathcal{L}^{(0)}, \mathcal{B}^{(0)}\}$ 
4  $\mathcal{R}$  is distributed to all clients  $k = 1, \dots, K$  *
5 for client  $k \leftarrow 1, \dots, K$  do  $\triangleright$  parallel loop
6 |  $D_k$  is data collected by client  $k$ 
7 end
8 for merge round  $m = 1, \dots, M$  do
9 | for client  $k = 1, \dots, K$  do  $\triangleright$  parallel loop
10 | |  $\mathcal{C}^{(m-1)}$  is received from the server *
11 | |  $\mathcal{C}_k^{(m)} \leftarrow \text{STrain-NeRF}(\mathcal{C}^{(m-1)}, \mathcal{R}, D_k, \Upsilon)$ 
   | |  $\triangleright \mathcal{C}_k^{(m)}$  contains  $\mathcal{L}_k^{(m)}, \mathcal{B}_k^{(m)}$ ; see Sec. 5.2
12 | |  $\mathcal{C}_k^{(m)}$  is transmitted to the server *
13 | end
14 | for  $k = 1, \dots, K$  do
15 | |  $\mathcal{W}_k^{(m)} \leftarrow \text{Recover}(\mathcal{L}_k^{(m)}, \mathcal{R}) \triangleright$  see Sec. 5.2
16 | |  $\theta_k^{(m)} \leftarrow \{\mathcal{W}_k^{(m)}, \mathcal{B}_k^{(m)}\}$ 
17 | end
18 |  $\theta^{(m)} \leftarrow \text{Combine}(\{\theta_k^{(m)}\}_{k=1, \dots, K}) \triangleright$  federated
   | averaging; see Sec. 5.1
19 |  $\mathcal{L}^{(m)} \leftarrow \text{Refactorise}(\mathcal{W}^{(m)}, \mathcal{R}) \triangleright$  extract
   | learnable parameters; see Sec. 5.2
20 |  $\mathcal{C}^{(m)} \leftarrow \{\mathcal{L}^{(m)}, \mathcal{B}^{(m)}\}$ 
21 end
22 return  $\theta^{(M)}$ 

```

---

## 5.1. Federated averaging for NeRF

Inspired by federated learning/averaging algorithms [12, 31], FedNeRF conducts  $M$  merging rounds to combine the models that are individually optimised by the  $K$  clients into an overall model. In each merging round, given  $K$  individual NeRF models  $\theta_k = \{\mathcal{W}_k, \mathcal{B}_k\}$ ,  $k = 1, \dots, K$ , where

$$\mathcal{W}_k = \{\mathbf{W}_{k,1}, \mathbf{W}_{k,2}, \dots\}, \quad \mathcal{B}_k = \{\mathbf{b}_{k,1}, \mathbf{b}_{k,2}, \dots\}, \quad (2)$$

we aim to compute a merged model  $\tilde{\theta} = \{\tilde{\mathcal{W}}, \tilde{\mathcal{B}}\}$ , where

$$\tilde{\mathcal{W}} = \{\tilde{\mathbf{W}}_1, \tilde{\mathbf{W}}_2, \dots\}, \quad \tilde{\mathcal{B}} = \{\tilde{\mathbf{b}}_1, \tilde{\mathbf{b}}_2, \dots\}. \quad (3)$$

The combination step (Step 18) in Alg. 2 obtains the merged weights by computing for each NeRF layer  $z$

$$\tilde{\mathbf{W}}_z = \frac{\sum_{k=1}^K |D_k| \mathbf{W}_{k,z}}{\sum_{k=1}^K |D_k|}, \quad (4)$$

where  $|D_k|$  is the size of the data collected by the  $k$ -th client. A similar weighted averaging is conducted for the bias parameters  $\tilde{\mathcal{B}}$ . The merged model  $\tilde{\theta}$  is then redistributed to each client for further refinement and merging.

## 5.2. Update compression for NeRF

In place of transferring the training images from the clients to the server, Alg. 2 conducts multiple exchanges of NeRF weights. Thus, it is vital to compress the amount of data that is transmitted in FedNeRF to be competitive in terms of bandwidth consumption. To this end, we adopt the update compression method of [4] to NeRF.

### 5.2.1 Reparameterisation

The first step (Step 2 in Alg. 2) is to linearly factorise the FC layers in the initial model. Via singular value decomposition (SVD), the  $z$ -th FC layer  $\mathbf{W}_z \in \mathbb{R}^{u \times v}$  becomes

$$\mathbf{W}_z = \mathbf{U}_z \mathbf{S}_z \mathbf{V}_z^\top, \quad (5)$$

where  $\mathbf{U}_z \in \mathbb{R}^{u \times u}$  contains the left singular vectors,  $\mathbf{V}_z \in \mathbb{R}^{v \times v}$  contains the right singular vectors, and  $\mathbf{S}_z \in \mathbb{R}^{u \times v}$  is

a diagonal matrix that contains the singular values, *i.e.*,

$$\mathbf{S}_z = \text{diag}(\mathbf{s}_z) \quad (6)$$

with vector  $\mathbf{s}_z$  of length  $\min(u, v)$ . Then,  $\mathbf{W}_z$  is truncated to rank  $r$ , where  $r \leq \min(u, v)$ , by computing

$$\mathbf{W}_z^r = \underbrace{\mathbf{U}_{z, :, 1:r} \text{diag}(\mathbf{s}_{z, 1:r})}_{\mathbf{L}_z} \underbrace{\mathbf{V}_{z, :, 1:r}^\top}_{\mathbf{R}_z}, \quad (7)$$

where  $\mathbf{U}_{z, :, 1:r}$  are the first- $r$  columns of  $\mathbf{U}_z$  (similarly for  $\mathbf{V}_{z, :, 1:r}$ ), and  $\mathbf{s}_{z, 1:r}$  are the first- $r$  elements of  $\mathbf{s}_z$ . Following [4],  $\mathbf{L}_z \in \mathbb{R}^{u \times r}$  becomes the *learnable* weights, while  $\mathbf{R}_z \in \mathbb{R}^{r \times v}$  are *frozen*. Performing the rank- $r$  truncation on all FC layers  $z = 1, 2, \dots$ , we have

$$\mathcal{L} = \{\mathbf{L}_1, \mathbf{L}_2, \dots\}, \quad \mathcal{R} = \{\mathbf{R}_1, \mathbf{R}_2, \dots\}. \quad (8)$$

The frozen parameters  $\mathcal{R}$  are shared with all clients prior to merging. Only  $\mathcal{L}$  (along with corresponding biases  $\mathcal{B}$ ) will be iteratively refined and exchanged between the server and clients during merging.

The value of  $r$  is guided by the amount of variance  $\alpha$  to be retained in  $\mathbf{W}_z^r$ . Specifically, we pick the smallest  $r$  s.t.

$$\frac{\sum_{i=1}^r s_{z,i}}{\sum_{i=1}^{\min(u,v)} s_{z,i}} \geq \alpha, \quad (9)$$

where  $s_{z,i}$  is the  $i$ -th singular value of  $\mathbf{W}_z$ . This implies that different FC layers in the NeRF will be truncated to different ranks. Section 6 will discuss the selection of  $\alpha$ .

### 5.2.2 Sparse training

Reparameterisation is conducted only once on the server side, then the learnable parameters are progressively updated by the clients through the rest of FedNeRF. In Step 11 of Alg. 2, client  $k$  refines the NeRF using data  $D_k$  by training for  $\Upsilon$  rounds on images  $I \in D_k$  in a similar way as in Sec. 3, except the training loss is backpropagated through the learnable parameters  $\mathcal{C}_k$  to update them only, leaving the frozen parameters  $\mathcal{R}$  unchanged.

### 5.2.3 Model recovery and re-factorisation

After the clients individually update the learnable parameters, the individual NeRFs are recovered

$$\mathcal{C}_k = \{\mathcal{L}_k, \mathcal{B}_k\} \mapsto \theta_k = \{\mathcal{W}_k, \mathcal{B}_k\} \quad (10)$$

in Steps 14 to 17 by recomputing each FC layer as

$$\mathbf{W}_{k,z} = \mathbf{L}_{k,z} \mathbf{R}_z. \quad (11)$$

After federated averaging in Step 18, the combined NeRF is refactorised to extract updated  $\mathcal{L} = \{\tilde{\mathbf{L}}_1, \tilde{\mathbf{L}}_2, \dots\}$  in Step 19 by solving for each FC layer

$$\tilde{\mathbf{L}}_z = \underset{\Gamma \in \mathbb{R}^{u \times r}}{\text{argmin}} \|\tilde{\mathbf{W}}_z - \Gamma \mathbf{R}_z\|_F, \quad (12)$$

which can be achieved via a linear solver. Alternatively, by recognising that the process (4) is linear, the FC layers of the merged NeRF are already factorisable by  $\mathcal{R}$  by default. Thus, Steps 18 and 19 for the weights can be simultaneously achieved by averaging the updated learnable layers

$$\tilde{\mathbf{L}}_z = \frac{\sum_{k=1}^K |D_k| \mathbf{L}_{k,z}}{\sum_{k=1}^K |D_k|}. \quad (13)$$

## 5.3. Bandwidth usage

Considering the lines marked with \* in Alg. 2, the total amount of data transferred in FedNeRF is

$$B_{\text{FedNeRF}} = K(|\mathcal{R}| + 2M|\mathcal{C}|), \quad (14)$$

where  $|\mathcal{R}|$  and  $|\mathcal{C}|$  are respectively the size in bytes of the frozen and learnable parameters of the NeRF model. The sizes can be reduced using standard file zipping methods.

The compression ratio CR achieved by FedNeRF over the baseline method is thus

$$\text{CR} = B_{\text{baseline}} / B_{\text{FedNeRF}}, \quad (15)$$

where higher CR means more economical bandwidth utilisation by FedNeRF. Of course, CR is inversely related to variance  $\alpha$ , which in turn is directly related to the representation power of the NeRF. Sec. 6 will examine the trade-off.

## 6. Experiments

We conduct a set of experiments to demonstrate that NeRFs can be learned in a federated manner. This section describes our experimental setup and details the datasets, evaluation metrics and implementation.

### 6.1. Experimental setup

**Datasets.** First, our technique is applied to a range of the real (horns, fern) and synthetic (lego, drums, materials, ship) single-object scenes used in the original NeRF paper [13]. This is done to validate that the structure of NeRFs is amenable to this federated training with update compression. To demonstrate the data compression capabilities of FedNeRF, we use a set of 1000 training images generated at random poses from the lego scene, dubbed the lego\_x1 dataset. Note that the choice of 1000 images is relatively arbitrary – the idea is to use this as a proof-of-concept larger dataset from readily-available data to demonstrate that compression is possible. As such, the compression ratio results would vary significantly with different image counts.

Finally, to investigate the performance of FedNeRF in an outdoor scene, we use the building dataset from Mega-NeRF [22].

**Evaluation metrics.** Following [13], we use the following metrics: image loss, learned perceptual image patch similarity (LPIPS) [30], structural similarity (SSIM) [23], and peak signal-to-noise ratio (PSNR).

**Baselines.** For all of our experiments, an initial network  $\theta^{(0)}$  is trained on a subset of the data. Given  $\theta^{(0)}$ , FedNeRF (Alg. 2) and the baseline (Alg. 1) were both executed and compared. This is especially an appropriate experimental setting for multi-round/lifelong learning campaigns, which is a key potential application of FedNeRF.

**Implementation.** For the synthetic scenes, all initial  $\theta^{(0)}$  were trained for 20 000 iterations on  $\frac{1}{5}$  of the original data, chosen randomly. The baseline method was then trained for  $T = 20\,000$  more iterations on the remaining  $\frac{4}{5}$ . FedNeRF was trained with update compression similarly from  $\theta^{(0)}$  for  $M = 20$  and  $\Upsilon = 1000$  with  $K = 4$  clients, each receiving  $\frac{1}{4}$  of the remaining  $\frac{4}{5}$ . The images for the clients were split such that the views were interspersed for these proof-of-concept experiments – further investigation into non-IID partitioning is left as future work. The same setting was followed for the real scenes, except with  $T = 25\,000$  for initial and baseline, and  $M = 25$  and  $\Upsilon = 1000$  for FedNeRF. In each experiment,  $\alpha = 90\%$ .

The settings above mean that the number of iterations *per client* for FedNeRF was the same as the number of iterations for the baseline *i.e.*, that  $M\Upsilon = T$ . While this meant that the cumulative iterations across all clients  $KM\Upsilon$  of FedNeRF was higher than the baseline’s  $T$ , the setting was justified since the clients ran in parallel. Of course each client operated on only a quarter of the data available to the baseline. In any case, we have tested the setting where  $KM\Upsilon = T$ , which yielded only slightly lower accuracy for FedNeRF.

For the `lego_x1` scene, three experiments as above were run by varying  $\alpha$  and  $M$  – one maximising network quality with minimal compression ( $\alpha = 90\%$ ,  $M = 20$ ), one maximising bandwidth compression ( $\alpha = 75\%$ ,  $M = 4$ ), and one balanced experiment in between ( $\alpha = 80\%$ ,  $M = 10$ ).

Similar experiments to the `lego_x1` dataset were undertaken for the building dataset. A single cell was trained on a section of the scene using Mega-NeRF’s spatial partitioning regime. The network structure was similar to that of standard NeRF, with the addition of per-image learned appearance embedding that were client specific. The training set for the single cell included all pixels from the whole scene which intersect the cell’s area. The initial model  $\theta^{(0)}$  was trained for 20 000 iterations on 320 images, with baseline being trained for a further  $T = 80\,000$  iterations. For FedNeRF,  $M$  was varied (160, 80, 20) with  $\Upsilon = T/M$ , and  $K = 2$  with each client having 800 images.

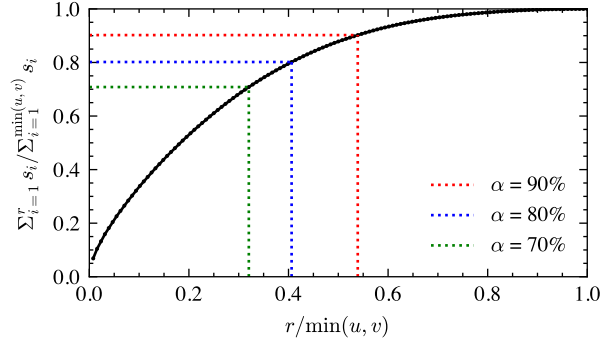


Figure 3. Representative plot of normalised cumulative sum of singular values  $s$  against  $r$  for layers in a NeRF. Most of the fully-connected layers exhibit this elbow-shaped characteristic, while a small number are closer to a linear relation.  $\alpha$  is as in Eq. (9).

**Hyperparameter settings.** The hyperparameters that affect the structure of the NeRF networks (number of layers, dimensions of layers, etc.) were selected to be similar to those used in the original papers [13, 22].

The graph in Fig. 3 informed the selection of  $\alpha$ . Setting  $\alpha$  to 70%–90% could produce large savings in parameter counts for most layers. Initial experiments indicated that values of  $\alpha < 70\%$  start to cause training to fail.

The same optimisation configuration is used for all experiments as in the original papers. The optimisers’ states are reset after training of the initial network for both baseline and FedNeRF. The optimiser is not reset for each training round between merges for the federated experiments.

Our focus was not to beat the synthesis quality of NeRF and Mega-NeRF as reported in [13, 22] (and as we are not altering the network structure, we do not believe this to be possible), but instead show that in some cases FedNeRF was able to converge faster than the baseline for a given number of training iterations. As such, the training iteration counts here were lower than what is used traditionally, but sufficient to produce good-quality images and allow for comparison of the techniques.

## 6.2. Results and discussion

The results in Tab. 1 for the real-world object scenes with one validation image each and Fig. 4 for the synthetic scenes with 200 validation images each show that the internal structure of these NeRFs are capable of being learned in a federated way, and are amenable to update compression. In fact, for every metric for every scene other than LPIPS for the `fern` scene, our FedNeRF method both improved on the initial network and outperformed the baseline network, which demonstrates that our method results in faster convergence than centralised training for these circumstances.

The results presented in Fig. 5 and Tab. 3 on the `lego_x1` dataset show that FedNeRF both uses less bandwidth and achieves better quality faster than the baseline approach.

Table 1. Validation results for federated learning of real-world single object scenes. Lower/higher better is indicated by ▼/▲ respectively.

Scene	Loss ▼			LPIPS ▼			SSIM ▲			PSNR ▲		
	Init.	Base.	Fed.	Init.	Base.	Fed.	Init.	Base.	Fed.	Init.	Base.	Fed.
fern	0.0096	0.0055	0.0055	0.4951	0.4756	0.4841	0.5832	0.6406	0.6426	20.18	22.58	22.64
horns	0.0048	0.0046	0.0039	0.5092	0.4862	0.4836	0.6520	0.6653	0.6836	23.20	23.41	25.36

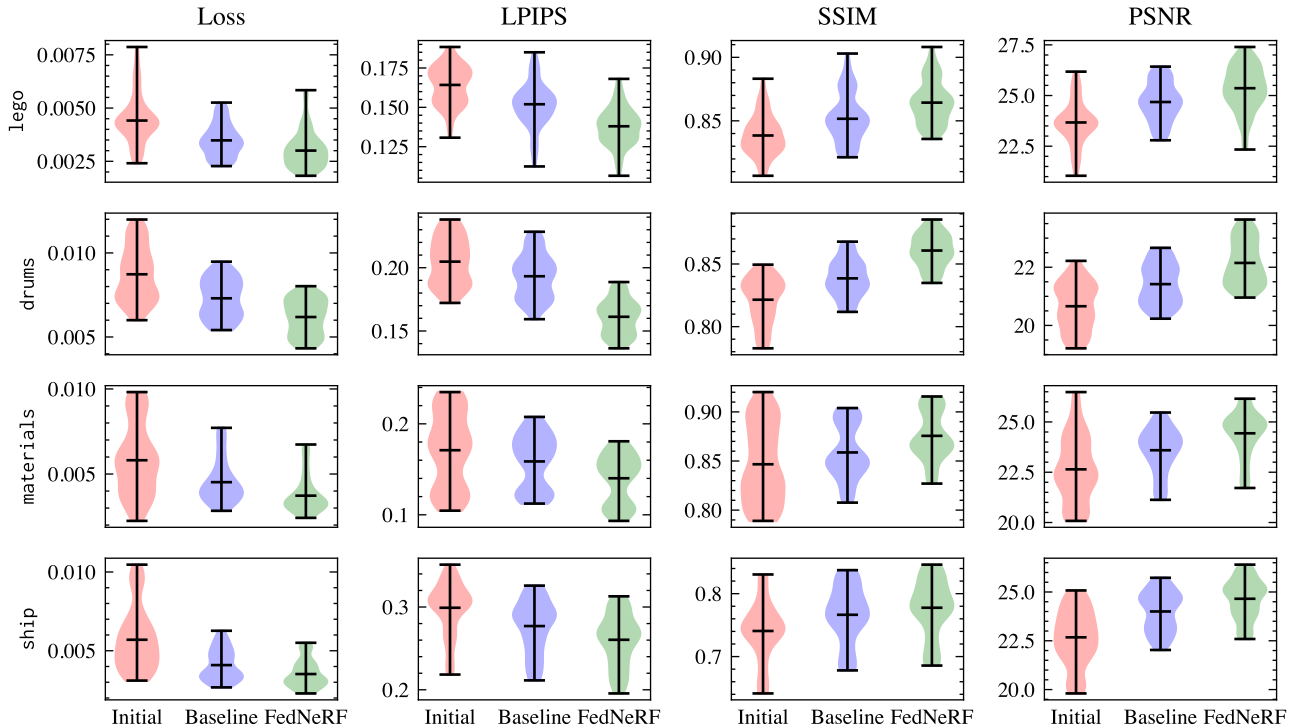


Figure 4. Validation results for the federated learning of synthetic single-object NeRF scenes. For loss and LPIPS lower is better, and for SSIM and PSNR higher is better. Our method is shown in green, compared to the baseline approach shown in blue.

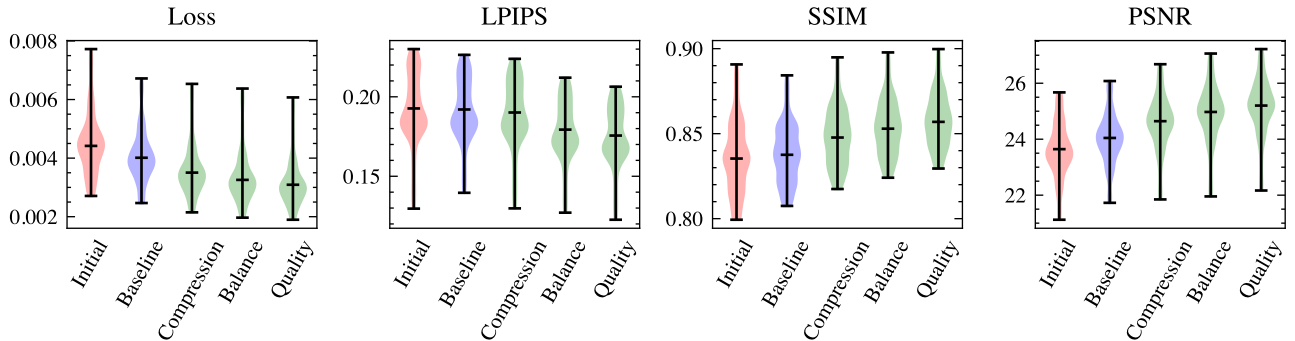


Figure 5. Validation results for the federated learning of higher image count synthetic NeRF scene lego\_x1. For loss and LPIPS lower is better, and for SSIM and PSNR higher is better. Our method is shown in green, compared to the baseline approach shown in blue.

The improved quality is clear in the qualitative results in Figs. 6 and 7.

In the outdoor scene case, our results in Tab. 2 that FedNeRF consistently shows improvements over the initial network, but in contrast to the previous results, it does not con-

verge faster than the baseline network. Examining the qualitative results shown in Fig. 7 highlight the significance of the improvements over the initial network, though, where the outputs of FedNeRF are much more suitable to a range of tasks like mapping and exploration. Additionally, Fed-

Table 2. Mean validation results for federated learning of a single cell of the building Mega-NeRF scene. Lower/higher better is indicated by ▼/▲ respectively. The dataset already uses JPEG-encoded images, so the compression ratios presented include this factor.  $\alpha$  is % variance retained as in (9).  $M$  is number of merges. CR is compression ratio.

Experiment	$\alpha$	$M$	CR	LPIPS ▼			SSIM ▲			PSNR ▲		
				Init.	Base.	Fed.	Init.	Base.	Fed.	Init.	Base.	Fed.
Quality	90%	160	1.00	0.7274	0.6532	0.7057	0.3370	0.3871	0.3608	17.14	18.58	17.89
Balance	80%	80	2.39			0.7398			0.3564			17.71
Compression	75%	20	10.33			0.7389			0.3558			17.72

Table 3. Compression ratio results for federated learning of higher image count synthetic NeRF scene lego\_x1. JPEG compression with 90% quality is used on the original PNG images, resulting in images c. 1/4 the size.  $\alpha$  is % variance retained as in (9).  $M$  is number of merges.

Experiment	$\alpha$	$M$	Compression Ratio	
			PNG	JPEG
Quality	90%	20	5.96	1.49
Balance	80%	10	15.29	3.82
Compression	75%	4	40.11	10.03

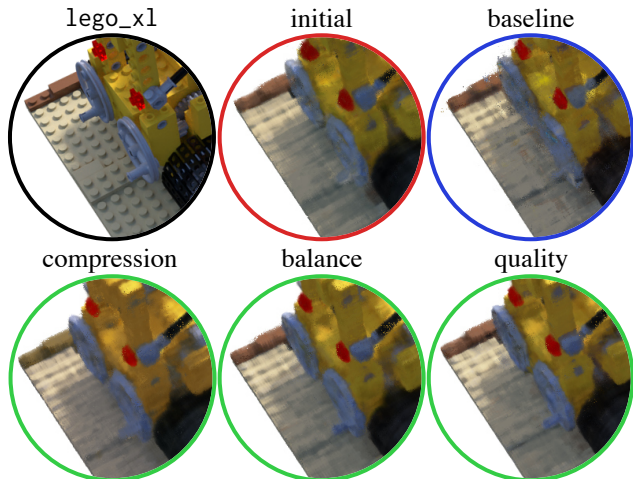


Figure 6. Close-up qualitative results for the single object lego\_x1, demonstrating the improved results of FedNeRF.

NeRF still exhibits significant bandwidth savings, and potential privacy improvements, and makes better use of the clients’ compute via parallelisation.

## 7. Conclusions and future work

In this paper, we present FedNeRF, a novel federated learning algorithm to train a NeRF in a parallel and distributed manner across multiple compute nodes without pooling the data. Our results show that the structure of NeRF is amenable to optimisation across multiple compute nodes, where each node tunes the model using an independent set of image observations of the overall scene. The up-

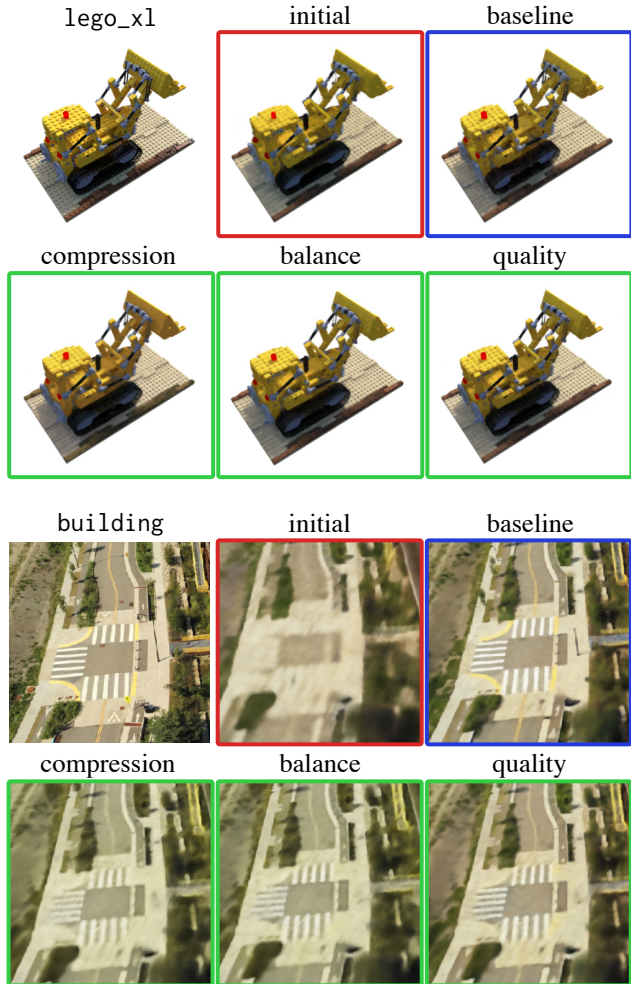


Figure 7. Qualitative results for the single object lego\_x1 and outdoor building scenes.

date compression method in FedNeRF was able to reduce the bandwidth consumption by more than 90% in certain cases without affecting the accuracy of the resulting NeRF.

These experiments demonstrate that FedNeRF works as a proof-of-concept, and valuable future work would involve testing more “real-world” experimental settings, including non-IID data partitioning, multiple data collection rounds, and more complex scenes with higher image counts.



## References

- [1] Alham Fikri Aji and Kenneth Heafield. Sparse Communication for Distributed Gradient Descent. In *Proceedings of the 2017 Conference on Empirical Methods in Natural Language Processing*, pages 440–445, Copenhagen, Denmark, Sept. 2017. Association for Computational Linguistics. 3
- [2] Jonathan T. Barron, Ben Mildenhall, Matthew Tancik, Peter Hedman, Ricardo Martin-Brualla, and Pratul P. Srinivasan. Mip-NeRF: A Multiscale Representation for Anti-Aliasing Neural Radiance Fields. In *2021 IEEE/CVF International Conference on Computer Vision (ICCV)*, pages 5835–5844, Montreal, QC, Canada, Oct. 2021. IEEE. 2
- [3] Nader Bouacida, Jiahui Hou, Hui Zang, and Xin Liu. Adaptive Federated Dropout: Improving Communication Efficiency and Generalization for Federated Learning. In *IEEE INFOCOM 2021 - IEEE Conference on Computer Communications Workshops (INFOCOM WKSHPS)*, pages 1–6, May 2021. 3
- [4] Bo Chen, Ali Bakhshi, Gustavo Batista, Brian Ng, and Tat-Jun Chin. Update Compression for Deep Neural Networks on the Edge. Apr. 2022. 3, 4, 5
- [5] Yang Chen, Xiaoyan Sun, and Yaochu Jin. Communication-Efficient Federated Deep Learning With Layerwise Asynchronous Model Update and Temporally Weighted Aggregation. *IEEE Transactions on Neural Networks and Learning Systems*, 31(10):4229–4238, Oct. 2020. 3
- [6] Dzung Doan, Yasir Latif, Tat-Jun Chin, Yu Liu, Thanh-Toan Do, and Ian Reid. Scalable Place Recognition Under Appearance Change for Autonomous Driving. In *2019 IEEE/CVF International Conference on Computer Vision (ICCV)*, pages 9318–9327, Seoul, Korea (South), Oct. 2019. IEEE. 1, 3
- [7] Jakub Konečný, Brendan McMahan, and Daniel Ramage. Federated Optimization: Distributed Optimization Beyond the Datacenter, Nov. 2015. 2
- [8] Jakub Konečný, H. Brendan McMahan, Felix X. Yu, Peter Richtárik, Ananda Theertha Suresh, and Dave Bacon. Federated Learning: Strategies for Improving Communication Efficiency, Oct. 2017. 3
- [9] Yujun Lin, Song Han, Huizi Mao, Yu Wang, and Bill Dally. Deep Gradient Compression: Reducing the Communication Bandwidth for Distributed Training. In *International Conference on Learning Representations*, Feb. 2022. 3
- [10] Ricardo Martin-Brualla, Noha Radwan, Mehdi S. M. Sajjadi, Jonathan T. Barron, Alexey Dosovitskiy, and Daniel Duckworth. NeRF in the Wild: Neural Radiance Fields for Unconstrained Photo Collections. In *2021 IEEE/CVF Conference on Computer Vision and Pattern Recognition (CVPR)*, pages 7206–7215, June 2021. 1, 2
- [11] Patrick McEnroe, Shen Wang, and Madhusanka Liyanage. A Survey on the Convergence of Edge Computing and AI for UAVs: Opportunities and Challenges. *IEEE Internet of Things Journal*, 9(17):15435–15459, Sept. 2022. 1, 2, 3
- [12] Brendan McMahan, Eider Moore, Daniel Ramage, Seth Hampson, and Blaise Aguera y Arcas. Communication-Efficient Learning of Deep Networks from Decentralized Data. In *Proceedings of the 20th International Conference on Artificial Intelligence and Statistics*, pages 1273–1282. PMLR, Apr. 2017. 2, 4
- [13] Ben Mildenhall, Pratul P. Srinivasan, Matthew Tancik, Jonathan T. Barron, Ravi Ramamoorthi, and Ren Ng. NeRF: Representing Scenes as Neural Radiance Fields for View Synthesis. Aug. 2020. 1, 2, 3, 5, 6
- [14] Jed Mills, Jia Hu, and Geyong Min. Communication-Efficient Federated Learning for Wireless Edge Intelligence in IoT. *IEEE Internet of Things Journal*, 7(7):5986–5994, July 2020. 3
- [15] Arthur Moreau, Nathan Piasco, Dzmitry Tsishkou, Bogdan Stanculescu, and Arnaud de La Fortelle. LENS: Localization enhanced by NeRF synthesis. Oct. 2021. 2
- [16] M. G. Sarwar Murshed, Christopher Murphy, Daqing Hou, Nazar Khan, Ganesh Ananthanarayanan, and Faraz Hussain. Machine Learning at the Network Edge: A Survey. *ACM Computing Surveys*, 54(8):170:1–170:37, Oct. 2021. 1
- [17] Daniel Rebain, Wei Jiang, Soroosh Yazdani, Ke Li, Kwang Moo Yi, and Andrea Tagliasacchi. DeRF: Decomposed Radiance Fields. In *2021 IEEE/CVF Conference on Computer Vision and Pattern Recognition (CVPR)*, pages 14148–14156, Nashville, TN, USA, June 2021. IEEE. 2
- [18] Christian Reiser, Songyou Peng, Yiyi Liao, and Andreas Geiger. KiloNeRF: Speeding up Neural Radiance Fields with Thousands of Tiny MLPs. In *2021 IEEE/CVF International Conference on Computer Vision (ICCV)*, pages 14315–14325, Montreal, QC, Canada, Oct. 2021. IEEE. 2
- [19] Felix Sattler, Simon Wiedemann, Klaus-Robert Müller, and Wojciech Samek. Sparse Binary Compression: Towards Distributed Deep Learning with minimal Communication. In *2019 International Joint Conference on Neural Networks (IJCNN)*, pages 1–8, July 2019. 3
- [20] Felix Sattler, Simon Wiedemann, Klaus-Robert Müller, and Wojciech Samek. Robust and Communication-Efficient Federated Learning From Non-i.i.d. Data. *IEEE Transactions on Neural Networks and Learning Systems*, 31(9):3400–3413, Sept. 2020. 3
- [21] Matthew Tancik, Vincent Casser, Xinchun Yan, Sabeek Pradhan, Ben Mildenhall, Pratul P. Srinivasan, Jonathan T. Barron, and Henrik Kretzschmar. Block-NeRF: Scalable Large Scene Neural View Synthesis, Feb. 2022. 1, 2
- [22] Haithem Turki, Deva Ramanan, and Mahadev Satyanarayanan. Mega-NeRF: Scalable Construction of Large-Scale NeRFs for Virtual Fly-Throughs, Mar. 2022. 1, 2, 3, 6
- [23] Zhou Wang, A.C. Bovik, H.R. Sheikh, and E.P. Simoncelli. Image quality assessment: From error visibility to structural similarity. *IEEE Transactions on Image Processing*, 13(4):600–612, Apr. 2004. 6
- [24] Frederik Warburg, Søren Hauberg, Manuel López-Antequera, Pau Gargallo, Yubin Kuang, and Javier Civera. Mapillary Street-Level Sequences: A Dataset for Lifelong Place Recognition. In *2020 IEEE/CVF Conference on Computer Vision and Pattern Recognition (CVPR)*, pages 2623–2632, June 2020. 3
- [25] Dingzhu Wen, Ki-Jun Jeon, and Kaibin Huang. Federated Dropout—A Simple Approach for Enabling Federated

- Learning on Resource Constrained Devices. *IEEE Wireless Communications Letters*, 11(5):923–927, May 2022. 3
- [26] Yuanbo Xiangli, Linning Xu, Xingang Pan, Nanxuan Zhao, Anyi Rao, Christian Theobalt, Bo Dai, and Dahua Lin. BungeeNeRF: Progressive Neural Radiance Field for Extreme Multi-scale Scene Rendering, July 2022. 1, 2
- [27] Jinjin Xu, Wenli Du, Yaochu Jin, Wangli He, and Ran Cheng. Ternary Compression for Communication-Efficient Federated Learning. *IEEE Transactions on Neural Networks and Learning Systems*, 33(3):1162–1176, Mar. 2022. 3
- [28] Lin Yen-Chen, Pete Florence, Jonathan T. Barron, Alberto Rodriguez, Phillip Isola, and Tsung-Yi Lin. INeRF: Inverting Neural Radiance Fields for Pose Estimation. Aug. 2021. 2
- [29] Kai Zhang, Gernot Riegler, Noah Snaveley, and Vladlen Koltun. NeRF++: Analyzing and Improving Neural Radiance Fields, Oct. 2020. 2
- [30] Richard Zhang, Phillip Isola, Alexei A. Efros, Eli Shechtman, and Oliver Wang. The Unreasonable Effectiveness of Deep Features as a Perceptual Metric. In *2018 IEEE/CVF Conference on Computer Vision and Pattern Recognition*, pages 586–595, Salt Lake City, UT, June 2018. IEEE. 6
- [31] Hangyu Zhu, Jinjin Xu, Shiqing Liu, and Yaochu Jin. Federated learning on non-IID data: A survey. *Neurocomputing*, 465:371–390, Nov. 2021. 4